International Journal of
Molecular Sciences

MDPI

Article

Sexual Dimorphism of Skeletal Muscle in a Mouse Model of Breast Cancer: A Functional and Molecular Analysis

Lauren E. Rentz [1], Marcella A. Whetsell [1], Stuart A. Clayton [1], Alan D. Mizener [2], Ida Holásková [3,4], Matthew G. Chapa [2], Emily H. Hoblitzell [4], Timothy D. Eubank [2,4] and Emidio E. Pistilli [1,2,4,*]

1 Division of Exercise Physiology, Department of Human Performance, West Virginia University School of Medicine, Morgantown, WV 26506, USA; lauren.rentz@hsc.wvu.edu (L.E.R.); mwhetsell@hsc.wvu.edu (M.A.W.); saclayton@mix.wvu.edu (S.A.C.)
2 Cancer Institute, West Virginia University School of Medicine, Morgantown, WV 26506, USA; adm0049@mix.wvu.edu (A.D.M.); mgc00016@mix.wvu.edu (M.G.C.); tdeubank@hsc.wvu.edu (T.D.E.)
3 Office of Statistics, West Virginia Agriculture and Forestry Experiment Station, Davis College of Agriculture, Natural Resources and Design, West Virginia University, Morgantown, WV 26506, USA; ida.holaskova@mail.wvu.edu
4 Department of Microbiology, Immunology, and Cell Biology, West Virginia University School of Medicine, Morgantown, WV 26506, USA; ehoblize@hsc.wvu.edu
* Correspondence: epistilli2@hsc.wvu.edu; Tel.: +1-304-293-0291

Abstract: Breast cancer incidence in men is statistically rare; however, given the lack of screening in males, more advanced stages at initial diagnosis result in lower 5-year survival rates for men with breast cancer compared to women. A sexual dimorphism, with respect to the effect of tumor growth on cachexia incidence and severity, has also been reported across cancer types. The purpose of this study was to examine the sexual dimorphism of breast cancer as it pertains to skeletal muscle function and molecular composition. Using female and male transgenic PyMT mice, we tested the hypothesis that the isometric contractile properties and molecular composition of skeletal muscle would be differentially affected by breast tumors. PyMT tumor-bearing mice of each sex, corresponding to maximal tumor burden, were compared to their respective controls. RNA sequencing of skeletal muscle revealed different pathway alterations that were exclusive to each sex. Further, differentially expressed genes and pathways were substantially more abundant in female tumor mice, with only minimal dysregulation in male tumor mice, each compared to their respective controls. These differences in the transcriptome were mirrored in isometric contractile properties, with greater tumor-induced dysfunction in females than male mice, as well as muscle wasting. Collectively, these data support the concept of sexually dimorphic responses to cancer in skeletal muscle and suggest that these responses may be associated with the clinical differences in breast cancer between the sexes. The identified sex-dependent pathways within the muscle of male and female mice provide a framework to evaluate therapeutic strategies targeting tumor-associated skeletal muscle alterations.

Keywords: cachexia; muscle wasting; RNA sequencing; muscle function; fatigue

Citation: Rentz, L.E.; Whetsell, M.A.; Clayton, S.A.; Mizener, A.D.; Holásková, I.; Chapa, M.G.; Hoblitzell, E.H.; Eubank, T.D.; Pistilli, E.E. Sexual Dimorphism of Skeletal Muscle in a Mouse Model of Breast Cancer: A Functional and Molecular Analysis. *Int. J. Mol. Sci.* **2023**, *24*, 11669. https://doi.org/10.3390/ijms241411669

Academic Editor: Helene Dumond

Received: 27 June 2023
Revised: 17 July 2023
Accepted: 18 July 2023
Published: 19 July 2023

1. Introduction

Breast cancer is the most common newly diagnosed malignancy among both sexes and the fourth leading cause of cancer-related death worldwide [1]. Comparatively, breast cancer in men is rare but highly lethal, with incidence increasing in recent decades [2]. Despite major advances in diagnosis and treatment, the American Cancer Society estimates 297,790 new breast cancer diagnoses and 43,700 deaths in the US for 2023 alone; only 2800 of these cases, or less than 1%, represent cases in males [1]. Although breast cancer in women and men share many risk factors, five-year survival rates in men are up to 43% lower [3]. Unlike women, recommendations for men do not include routine screening examinations for breast cancer. When this lack of screening is combined with the absence

of early signs and symptoms of the disease, it results in more advanced stages of disease at first diagnosis [3,4].

The development of genetically modified mouse models has been instrumental in elucidating the understanding of early dissemination, progression, and metastasis in human breast cancer, as well as in validating human cancer genes, dysregulated signaling pathways, and therapeutic approaches [5–9]. The MMTV-PyMT FVB/NJ mouse strain has been extensively used to study mammary carcinoma formation and metastasis, with important clinical implications. The PyMT breast cancer model is similar to human breast cancer based on commonalities in the penetrance, frequency, and sites of metastases [7,10]. While the PyMT oncoprotein is not expressed in human breast tumor cells, it acts as a potent oncogene that is capable of activating oncogenic pathways that are also activated by human breast tumors; these pathways promote cell proliferation and accelerate growth to foster an aggressive tumor phenotype [7,11,12].

In female PyMT mice, spontaneous breast tumor growth begins at approximately four weeks of age and is characterized by four distinctly identifiable stages of tumor progression [11], which mirrors the pathology of human breast cancer with respect to hyperplasia, adenoma, and early to late carcinoma [8,9,11,12]. In contrast, male MMTV-PyMT mice display a delayed onset of tumor growth with lower penetrance of metastasis, resembling tumor growth profiles in men, which develop 5 to 10 years later than in women [13]. Gene expression profiling has revealed that PyMT mouse breast tumors model the luminal B molecular subtype of human breast cancer, with overexpression of the estrogen receptor (ER), progesterone receptor (PR), and human epidermal growth factor receptor 2 (Her2/neu) [7,10,13]. Overall, these observations reinforce that tumor progression in female and male PyMT mice recapitulates the complex stages and heterogeneity of breast cancer in humans.

Cancer-associated cachexia is a major paraneoplastic syndrome, in which the wasting of muscle and/or adipose tissue occurs at the expense of the host as a means to fuel tumor growth [14]. Muscle weakness and fatigue often ensue in concert with muscle wasting, despite separate mechanisms promoting muscle wasting vs. muscle fatigue [15]. Cachexia incidence and severity in breast cancer patients are significantly lower compared to other cancer types [16]. Our laboratory has suggested that early-stage breast cancer is associated with a clinically relevant phenotype of muscle fatigue in the absence of muscle wasting, which is supported by data from early-stage patients and mouse models of breast cancer [17,18]. Despite our data suggesting that breast cancer patients remain relatively weight-stable [18], persistent fatigue is among the most common symptoms reported by patients [19–21]. The presence of fatigue can reduce a patient's ability to tolerate vital cancer therapy and negatively impact quality of life, potentially reducing overall survival [22,23].

Across cancer types, there appears to be a sexual dimorphism with respect to the effects of tumor growth on muscle mass and functional properties, with men experiencing a greater degree of tissue wasting compared to women [24,25]. The purpose of the present study was to perform a deeper evaluation of the sexual dimorphism of breast cancer, specifically as it pertains to skeletal muscle function and molecular composition, utilizing the PyMT mouse model. Prior findings from our laboratory have identified altered gene and protein expression patterns, mitochondrial dysfunction, and lower ATP concentrations in the skeletal muscles of female patients with breast cancer, translating to impaired contractility and a more fatigable phenotype [17,18,26]. We tested the hypothesis that the isometric contractile properties and molecular composition of skeletal muscle would be differentially affected by breast tumors in female and male PyMT mice.

2. Results

2.1. Bulk RNA Sequencing

The characterization of breast tumor influence on the skeletal muscle of male and female PyMT mice using RNA sequencing is shown in Figure 1A–D. K-means clustering of the 2000 most variable genes revealed two clusters (out of a total of four) with sample

variability explained by sex, independent of tumor group, as seen in Figure 1A. These sex-dependent clusters included cluster A (511 genes), representing genes with greater expression in female groups, and cluster C (325 genes), representing genes with greater expression in male groups. Cluster B (629 genes) and cluster D (535 genes) mostly reflected the interaction between the main factors of sex and group, with cluster B reflecting genes upregulated in the muscles of female tumor (FT) mice compared to female control (FC) mice and cluster D reflecting genes downregulated in the muscles of FT mice compared to FC mice. Genes within these two clusters were not differentially expressed between the male groups. Table 1 shows the top 10 gene ontology (GO) pathways for each of the four clusters.

The first five components of the PCA were able to explain 72% of sample variance between the four study groups, with 59% being explained from the first two PCs alone (Figure 1B); the first five PCs explained 38%, 21%, 5%, 4%, and 4%, respectively. PC 1 was significantly correlated to the main factor of sex ($p = 1.95 \times 10^{-4}$); however, it was not until PC 5 that the main factor of tumor group was significantly correlated ($p = 0.0237$). The findings from this analysis suggest that the female groups (FC, FT) are well delineated by PCs 1 and 2, which represents most inter-group variance, whereas minimal variance exists between the male groups (MC, MT).

Figure 1C,D display DEGs with an FDR cutoff of 0.1 and a minimum fold change of 1 compared across the study groups. Figure 1C presents similarities and differences in the total number of differentially expressed genes between the study groups, whereas Figure 1D presents the number of differentially expressed genes that were either upregulated or downregulated. The greatest number of differentially regulated genes existed between the muscles of MT and FT mice (8936 genes); however, less than half of these genes (4277) can be considered sexually dimorphic, demonstrating differential expression between males and females of both the control (MC-FC) and tumor (MT-FT) groups. It should be noted that 4659 DEGs existed between the tumor groups (MT-FT) that did not exist between the control groups (MC-FC). Further, 7951 genes were dysregulated in FT mice compared to FC, while only 40 genes were dysregulated in MT compared to MC mice, suggesting a lower effect of breast tumor growth in MT mice (Figure 1C,D). Interestingly, of the 40 differentially expressed genes between MT and MC mice, only 1 gene was unique to this comparison (*Ube2l6*, $\log_2$ fold change 1.3725; $p = 0.0755$). Only 11 of the 40 DEGs in males were not differentially expressed in females; these genes were *Nbdy*, *Tubb6*, *Csrp3*, *Col20a1*, *Cyth4*, *Adprh*, *Ube2l6*, *Myl4*, *Klhl40*, *Hbb-bs*, and *Galnt5*. Further, 20 of the 40 DEGs in males were also dysregulated in females, but male and female controls were not different; *Mymk* was the only gene that differed in the directionality of change, showing downregulation in females and upregulation in males. Nine genes were differentially expressed in response to breast tumors in a consistent manner for both sexes, and they were not sexually dimorphic: *Alas2*, *Tent5c*, *Ppp1r3c*, *Sele*, *Arrb1*, *Txnip*, *Slc4a1*, *Ctss*, and *Cox7c*.

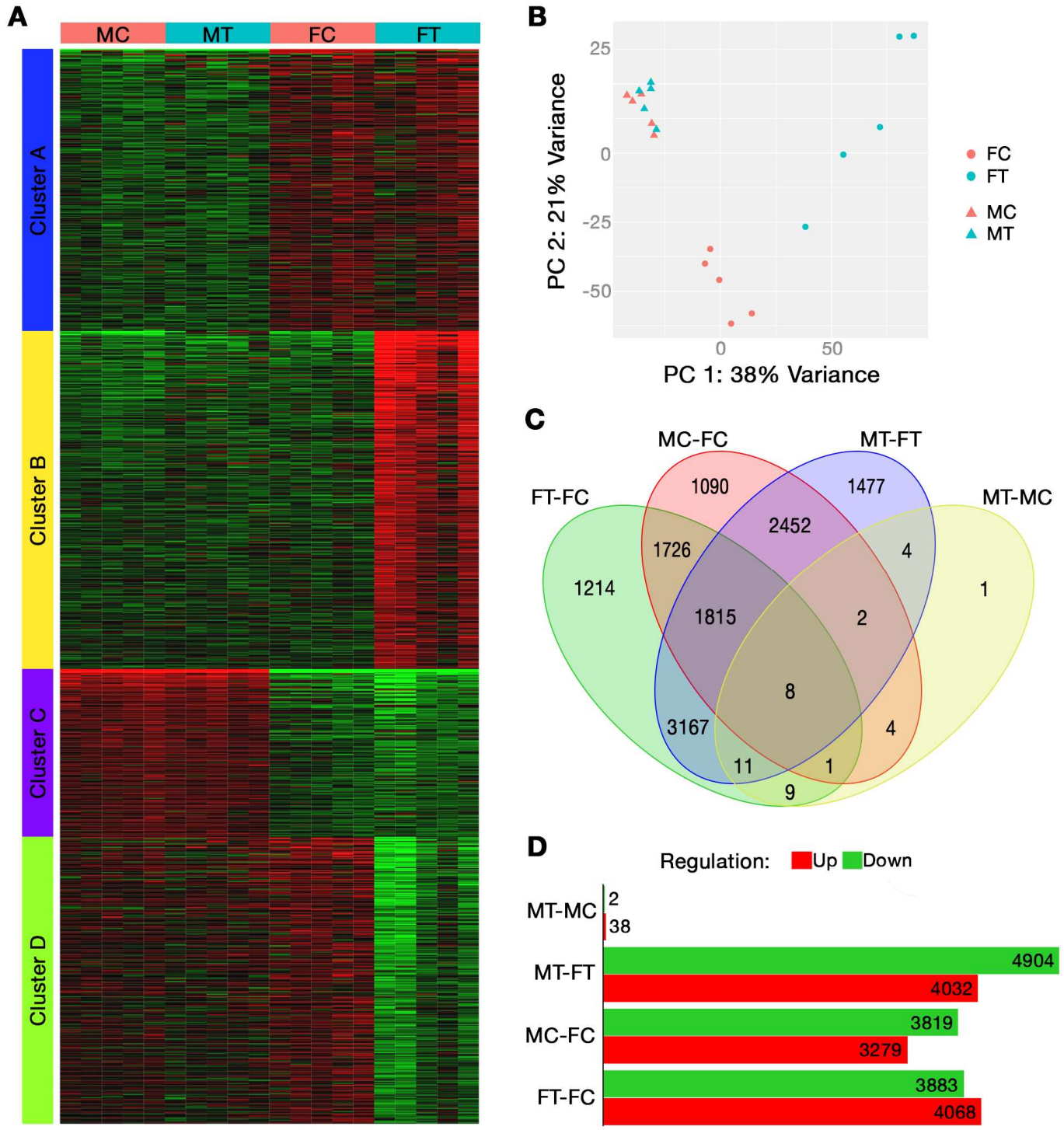

Figure 1. (**A**–**D**). Breast cancer influence on skeletal muscle of male and female PyMT mice. RNA sequencing evaluation of gene expression in the tibialis anterior (TA) muscle, performed using $n = 5$ mice per sample group. (**A**) Clustered heatmap of gene expression for the 2000 most variable genes; red represents greater expression and green represents lesser expression, (**B**) principal component analysis plot comparing sample eigenvectors for the first two principal components, (**C**) Venn diagram of differentially expressed genes with an FDR of 0.1 and minimum fold change of 1.0, (**D**) up- and downregulated differentially expressed genes (FDR of 0.1 and min fold change of 1.0) across study groups. FC, female control; FT, female tumor; MC, male control; MT, male tumor; PC, principal component.

Table 1. Top differentially expressed pathways in cluster analysis.

Cluster	Adj. *p*-Value	# Genes	Pathways	Gene Ontology
A	1.19×10^{-3}	44	Extracellular region	Cellular Component
	1.19×10^{-3}	3	Hemoglobin complex	Cellular Component
	1.50×10^{-3}	3	Haptoglobin binding	Molecular Function
	1.62×10^{-3}	3	Haptoglobin–hemoglobin complex	Cellular Component
	7.09×10^{-3}	30	Extracellular space	Cellular Component
	7.09×10^{-3}	3	Troponin complex	Cellular Component
	7.09×10^{-3}	15	Collagen-containing extracellular matrix	Cellular Component
	7.23×10^{-3}	4	Transition between fast and slow fiber	Biological Process
	7.23×10^{-3}	28	Positive regulation of immune system process	Biological Process
	7.30×10^{-3}	3	Oxygen carrier activity	Molecular Function
B	1.53×10^{-14}	132	Immune system process	Biological Process
	3.38×10^{-14}	136	Response to external stimulus	Biological Process
	7.07×10^{-13}	88	Defense response	Biological Process
	5.08×10^{-12}	40	Leukocyte migration	Biological Process
	2.28×10^{-11}	30	Leukocyte chemotaxis	Biological Process
	3.04×10^{-11}	35	Cell chemotaxis	Biological Process
	3.50×10^{-11}	22	Neutrophil migration	Biological Process
	3.50×10^{-11}	54	Inflammatory response	Biological Process
	3.65×10^{-11}	150	Response to organic substance	Biological Process
	4.94×10^{-11}	29	Myeloid leukocyte migration	Biological Process
C	1.22×10^{-5}	27	Monocarboxylic acid metabolic process	Biological Process
	1.76×10^{-4}	49	Small molecule metabolic process	Biological Process
	2.02×10^{-4}	31	Carboxylic acid metabolic process	Biological Process
	2.02×10^{-4}	31	Oxoacid metabolic process	Biological Process
	3.42×10^{-4}	29	Metal ion transport	Biological Process
	3.70×10^{-4}	20	Purine-containing compound metabolic process	Biological Process
	7.77×10^{-4}	40	Ion transport	Biological Process
	7.77×10^{-4}	34	Cation transport	Biological Process
	1.03×10^{-3}	27	Oxidoreductase activity	Molecular Function
	1.31×10^{-3}	18	Ribonucleotide metabolic process	Biological Process
D	1.30×10^{-37}	138	Extracellular region	Cellular Component
	3.71×10^{-32}	104	Extracellular space	Cellular Component
	5.10×10^{-27}	64	External encapsulating structure	Cellular Component
	5.10×10^{-27}	64	Extracellular matrix	Cellular Component
	2.66×10^{-22}	51	Collagen-containing extracellular matrix	Cellular Component
	2.44×10^{-20}	33	Extracellular matrix structural constituent	Molecular Function
	1.17×10^{-11}	196	System development	Biological Process
	1.26×10^{-11}	19	Collagen trimer	Cellular Component
	1.26×10^{-11}	9	Fibrillar collagen trimer	Cellular Component
	1.26×10^{-11}	9	Banded collagen fibril	Cellular Component

Data presented are the top 10 differentially expressed pathways from each of the four clusters from the clustering analysis, which considered the 2000 most variable genes. These k-means clusters tend to correspond to the following patterns: cluster A, greater expression in female groups, cluster B, greater expression in female tumor group only, cluster C, greater expression in male groups, and cluster D, lower rates of expression in female tumor group only. #, number; Adj, adjusted.

The top 10 upregulated and downregulated biological pathways in tumor mice compared to controls for each sex are reported in Table 2, which considers expression for all genes in the enrichment of GO pathways. Collectively, in FT compared to FC, 84 pathways were significantly downregulated and 17 significantly upregulated. In MT compared to MC, 16 pathways were significantly upregulated, while none were downregulated. Notably, the significantly affected pathways for each sex were entirely exclusive, including both up- and downregulated; this suggests no similar pathway alterations in response to tumor growth between males and females.

Table 2. Top dysregulated pathways in males and females.

Sex	Regulation	Pathways	Gene Ontology	Statistic	# Genes	Adj. *p*-Value
Female	Down	External encapsulating structure	Cellular Component	−7.348	363	1.4×10^{-10}
		Extracellular matrix	Cellular Component	−7.2978	362	1.4×10^{-10}
		Extracellular matrix structural constituent	Molecular Function	−7.236	111	4.1×10^{-9}
		Collagen-containing extracellular matrix	Cellular Component	−6.8648	277	2.1×10^{-9}
		Fibrillar collagen trimer	Cellular Component	−5.5438	10	7.5×10^{-4}
		Banded collagen fibril	Cellular Component	−5.5438	10	7.5×10^{-4}
		Mitochondrial inner membrane	Cellular Component	−5.4532	408	5.8×10^{-6}
		Extracellular matrix organization	Biological Process	−5.2292	241	2.0×10^{-4}
		Extracellular structure organization	Biological Process	−5.2292	241	2.0×10^{-4}
		External encapsulating structure organization	Biological Process	−5.2292	241	2.0×10^{-4}
	Up	Ribonucleoprotein complex biogenesis	Biological Process	6.2942	397	1.7×10^{-6}
		Ribosome biogenesis	Biological Process	5.7665	278	2.3×10^{-5}
		RRNA metabolic process	Biological Process	5.2363	210	2.9×10^{-4}
		RRNA processing	Biological Process	5.1772	203	3.0×10^{-4}
		Cytosolic ribosome	Cellular Component	4.8633	100	9.8×10^{-4}
		NcRNA metabolic process	Biological Process	4.6176	424	0.0027
		NcRNA processing	Biological Process	4.5756	352	0.0028
		Posttranscriptional regulation of gene expression	Biological Process	4.045	437	0.023
		Cytoplasmic translation	Biological Process	4.0078	93	0.035
		Autophagy	Biological Process	3.8234	390	0.041
Male	Up	Inflammatory response	Biological Process	4.9953	475	0.002
		Leukocyte migration	Biological Process	4.7888	264	0.0033
		Innate immune response	Biological Process	4.606	469	0.0045
		Cytokine-mediated signaling pathway	Biological Process	4.3149	279	0.014
		Myeloid leukocyte migration	Biological Process	4.1515	158	0.024
		Response to bacterium	Biological Process	4.0783	450	0.024
		Regulation of cell activation	Biological Process	3.8591	425	0.043
		Regulation of leukocyte activation	Biological Process	3.8372	391	0.043
		Tumor necrosis factor superfamily cytokine production	Biological Process	3.8201	136	0.043
		Regulation of tumor necrosis factor superfamily cytokine production	Biological Process	3.8201	136	0.043

Data presented are the top 10 upregulated and downregulated pathways in tumor mice compared to controls for each sex with an FDR of <0.05. #, number; Adj, adjusted.

The downregulated pathways that occurred only in female muscles in response to tumor growth were primarily those involving extracellular membrane structure, cell metabolism, and synaptic membranes. In addition to those listed in Table 2, other downregulated pathways in this group related to cell metabolism include GO Biological Process pathways for *cellular respiration* (statistic = −4.978, 195 genes, $p = 0.0005$), *oxidative phosphorylation* (statistic = −4.878, 115 genes, $p = 0.00068$), and *aerobic respiration* (statistic = −4.8502, 156 genes, $p = 0.00068$) and a GO Cellular Component pathway for the *respiratory chain complex* (statistic = −4.2996, 76 genes, $p = 0.00076$). Additional downregulated pathways involving synaptic membranes include GO Biological Process pathways for *synapse organization* (statistic = −4.8932, 370 genes, $p = 0.0005$) and *regulation of synapse structure or activity* (statistic = −4.1964, 203 genes, $p = 0.0068$), as well as GO Cellular Component pathways for the *presynaptic membrane* (statistic = −2.9267, 118 genes, $p = 0.033$) and *postsynaptic membrane* (statistic = −3.646, 202 genes, $p = 0.0031$).

Upregulated pathways in muscles of FT mice primarily reflected increased autophagic and protein synthesis-related mechanisms. In addition to those listed in Table 2, other upregulated pathways in this group include GO Biological Process pathways for *mRNA processing* (statistic = 3.7728, 419 genes, $p = 0.046$) and *process utilizing autophagic mechanisms* (statistic = 3.8234, 390 genes, $p = 0.041$), as well as GO Cellular Component pathways for the *vacuole* (statistic = 3.6718, 466 genes, $p = 0.044$), *nuclear speck* (statistic = 3.4796, 373 genes, $p = 0.046$), and *autophagosome* (statistic = 3.4558, 85 genes, $p = 0.046$).

Upregulated pathways in muscles from MT mice primarily reflected increased inflammatory activity, with mechanisms involving leukocytes and TNF-α. In addition to those listed in Table 2, other upregulated pathways in this group include GO Biological Process pathways for *granulocyte migration* (statistic = 3.7993, 103 genes, $p = 0.044$), *TNF-α production* (statistic = 3.7974, 134 genes, $p = 0.043$), *neutrophil migration* (statistic = 3.7915, 84 genes, $p = 0.045$), and *leukocyte differentiation* (statistic = 3.7127, 414 genes, $p = 0.044$).

KEGG pathways illustrating the fold change in the expression of relevant genes in tumor mice compared to controls for both sexes in the *cardiac muscle contraction* and *antigen processing and presentation* pathways are depicted in Figures 2 and 3, respectively. *Class I helical cytokine interactions and PPAR signaling*, *calcium signaling*, *oxidative phosphorylation*, and *mitophagy* KEGG pathways are depicted in Figures S1A–D, S2A,B, S3A,B and S4A,B, respectively.

To assess the consistency of the RNA sequencing data, MC mice were compared against FC mice for further evaluation of genes previously identified to be sexually dimorphic in mouse skeletal muscle [27]. The differential expression data between male and female controls for these genes are provided in Table S1. Nine of the eleven genes previously reported to represent the sexual dimorphism of skeletal muscles were differentially expressed in the present study between the male and female control groups (FDR < 0.1).

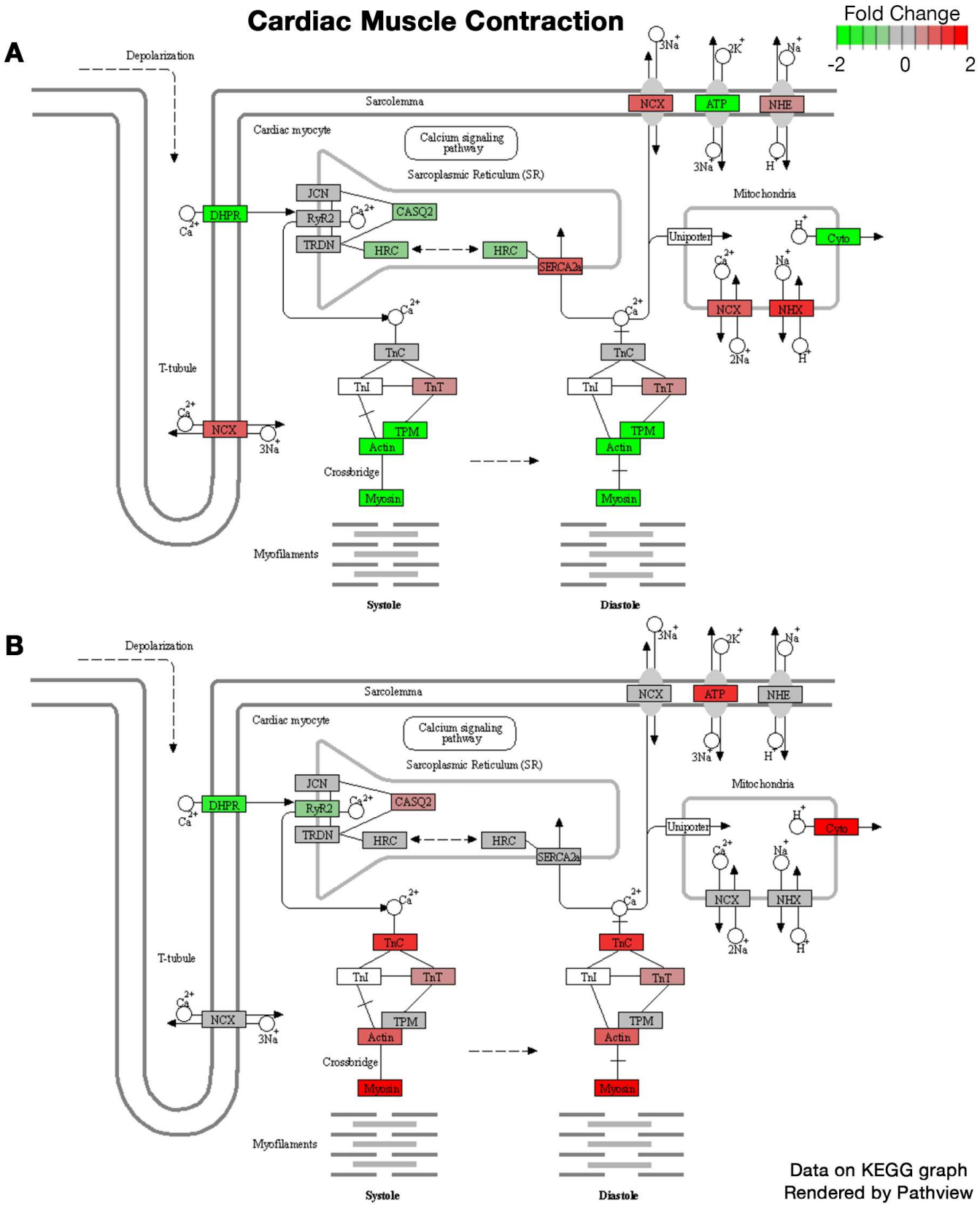

Figure 2. (**A**,**B**) Differential pathway expression of cardiac muscle contraction pathway. Figure modified from KEGG graphs rendered using Pathview. (**A**) Differential expression in female tumor mice compared to female controls. (**B**) Differential expression in male tumor mice compared to male controls. RNA sequencing was performed using $n = 5$ mice per sample group.

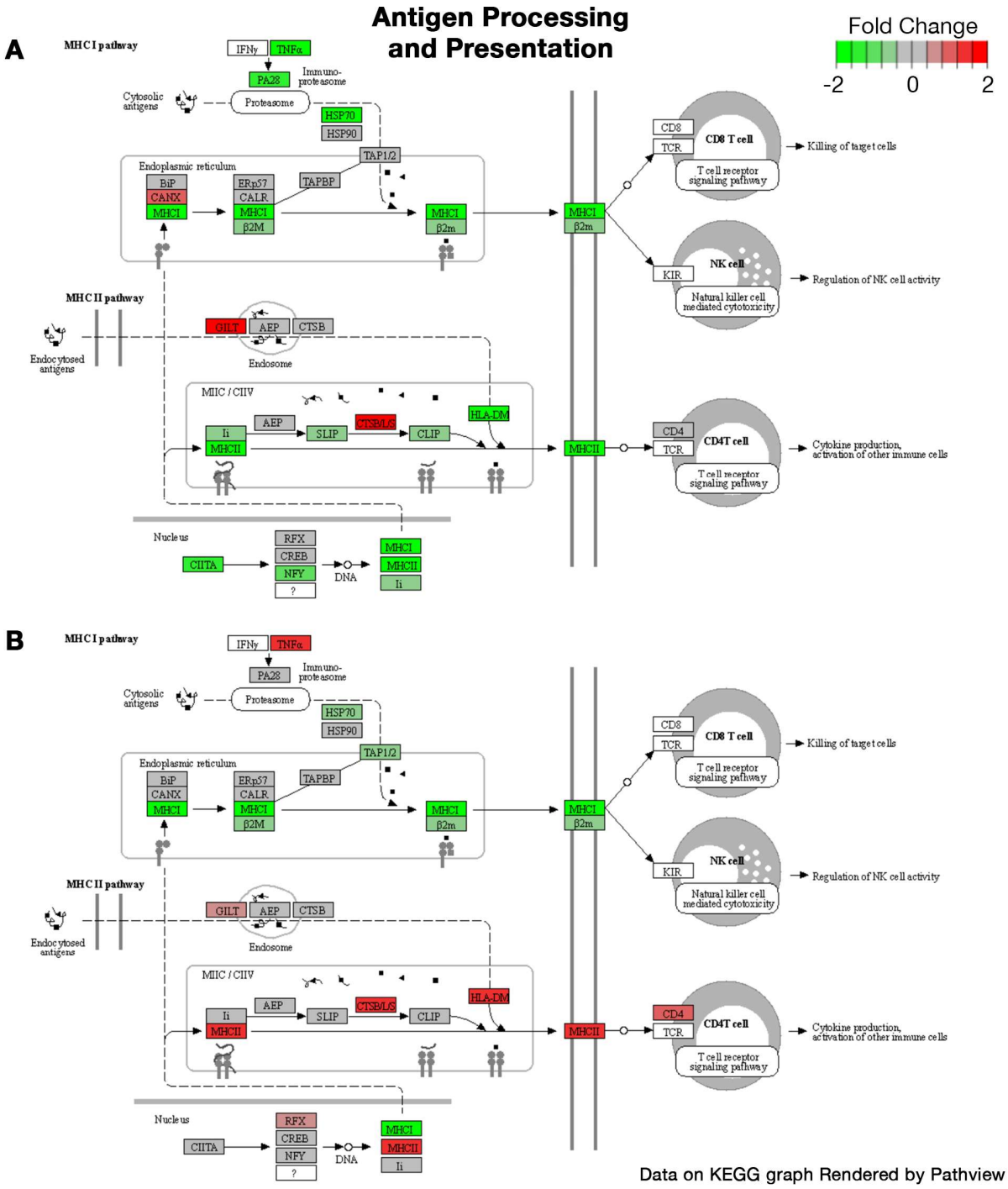

Figure 3. (**A**,**B**) Differential pathway expression of antigen processing and presentation. Figure modified from KEGG graphs rendered using Pathview. (**A**) Differential expression in female tumor mice compared to female controls. (**B**) Differential expression in male tumor mice compared to male controls. RNA sequencing was performed using $n = 5$ mice per sample group.

2.2. Skeletal Muscle Properties

Sample sizes of all ex-vivo muscle variables are included in Table S2.

Figure 4A–F depict the relationships between sex and tumor group on isometric contractile properties, including mixed model fixed effects, with additional physiological properties described in Table 3. Significantly lower extensor digitorum longus (EDL) weight (Figure 4A, $p = 0.0053$), cross sectional area (CSA; Figure 4B, $p = 0.0470$), tetanus force (Figure 4D, $p = 0.0057$), optional length (L_o) of the EDL muscle (Table 3, $p = 0.0203$), rate of

force development (RFD; Table 3, $p = 0.0372$), relaxation rate (RR; Table 3, $p = 0.0448$), maximal force (P_{max}) generated (Table 3, $p = 0.0076$), and absolute force–frequency (Figure 4F, $p = 0.0122$) existed in FT mice compared to FC mice, while no pairwise differences were observed between the male groups. Sex differences in control mice only existed for CSA (Figure 4B) and P_{max} (Table 3), though significant pairwise differences between MT and FT mice were widespread.

Table 3. Physiological properties of EDL muscle in male and female mice.

	Group LSM ± SE				Fixed Effect *p*-Values		
Variable	**Female Control**	**Female Tumor**	**Male Control**	**Male Tumor**	**ME of Sex**	**ME of Group**	**Sex*Group Interaction**
L_o [a,b]	11.63 ± 0.17	10.76 ± 0.21	11.01 ± 0.42	12.05 ± 0.20	0.2243	0.7577	**0.0018**
CT	22.5 ± 2.07	24.0 ± 2.61	26.0 ± 2.61	25.0 ± 1.69	0.3332	0.9136	0.5884
$\frac{1}{2}$ RT	35.0 ± 2.50	36.0 ± 3.16	26.0 ± 3.16	35.5 ± 2.49	0.1090	0.0792	0.1507
Twitch/CSA	56.5 ± 6.40	56.8 ± 8.10	42.0 ± 8.10	62.4 ± 6.25	0.5478	0.1664	0.1816
Tetanus/CSA	247.2 ± 17.0	247.6 ± 21.5	156.9 ± 21.5	199.6 ± 18.2	**0.0020**	0.2846	0.2924
RFD [a,b]	2069.5 ± 168.0	1286.0 ± 212.5	1700.4 ± 212.5	2341.1 ± 154.2	0.0814	0.7083	**0.0009**
RR [a,b]	−1048.2 ± 81.0	−683.1 ± 102.5	−1346.6 ± 115.7	−1306.1 ± 72.2	**<0.0001**	**0.0412**	0.0975
P_{min} [b]	54.4 ± 5.47	39.4 ± 6.92	58.1 ± 6.92	77.5 ± 5.85	**0.0033**	0.7289	**0.0130**
P_{max} [a,c]	256.8 ± 12.2	185.2 ± 15.4	201.1 ± 15.4	234.8 ± 13.01	0.8330	0.1924	**0.0012**
K_f	32.1 ± 1.96	35.3 ± 2.48	32.0 ± 2.48	28.8 ± 2.10	0.1623	0.9959	0.1759
h	2.45 ± 1.67	2.34 ± 2.11	4.19 ± 1.20	5.28 ± 0.18	0.1295	0.7430	0.6888

Data represent ex vivo physiological properties of the EDL muscle in male and female stage 4 tumor mice and age-matched controls. Group data are presented as least squares means (LSM) ± SE. Fixed effects are also presented for each model, with significant effects denoted in bold. Significant pairwise differences identified using Tukey's HSD are represented by superscripts for each variable and are denoted as follows: [a] female tumor vs. female control, [b] female tumor vs. male tumor, and [c] female control vs. male control; no pairwise differences existed between male tumor and male control groups. CSA, cross sectional area; CT, contraction time; K_f, half-frequency; h, hill coefficient; L_o, optimal length; ME, main effect; P_{max}, maximum force; P_{min}, minimum force; RFD, rate of force development; RR, rate of relaxation; RT, relaxation time

The force–frequency relationship is presented in Figure 4F. While the main effects of sex or group alone did not significantly affect force, significant interactions did exist for sex*group ($p = 0.0010$) and sex*group*frequency ($p = 0.0397$). These findings suggest vertical and lateral shifting of absolute forces in the force–frequency relationship between the four sample groups, indicating different trends in force production at a given frequency in FT-FC mice than in MT-MC mice. No differences were observed in the force–frequency relationship for any group when force at each frequency was normalized to maximal force output. Overall, these data suggest that breast tumor growth in female mice contributes to a significant reduction in EDL mass and absolute force output, whereas tumor-induced muscle contractility impairments were absent in male mice.

Body mass was significantly affected by sex (main effect: $p < 0.0001$) and group (main effect: $p < 0.0001$) and there was a significant interaction between sex*group ($p < 0.0001$). FT mice (39.8 ± 1.4 g) had a substantially greater body mass compared to FC mice (22.2 ± 1.6 g, $p < 0.0001$), with tumor mass contributing to this difference. No difference in body mass between the male groups was observed. The masses of individual muscles for each study group are represented in Figure 5. Significant main effects of sex ($p < 0.0001$) existed for all four muscles, while a main effect of tumor group only existed for the EDL muscle ($p = 0.0011$) and approached significance for the Tibialis Anterior muscle (TA; $p = 0.0592$), representing lower muscle weights in tumor groups. A sex*group interaction existed for all muscles aside from the soleus ($p = 0.1696$). Collectively, these data demonstrate that muscles from FT mice, but not MT mice, consistently demonstrate muscle wasting, relative to their respective controls, supporting the lower muscle isometric force output only in female mice.

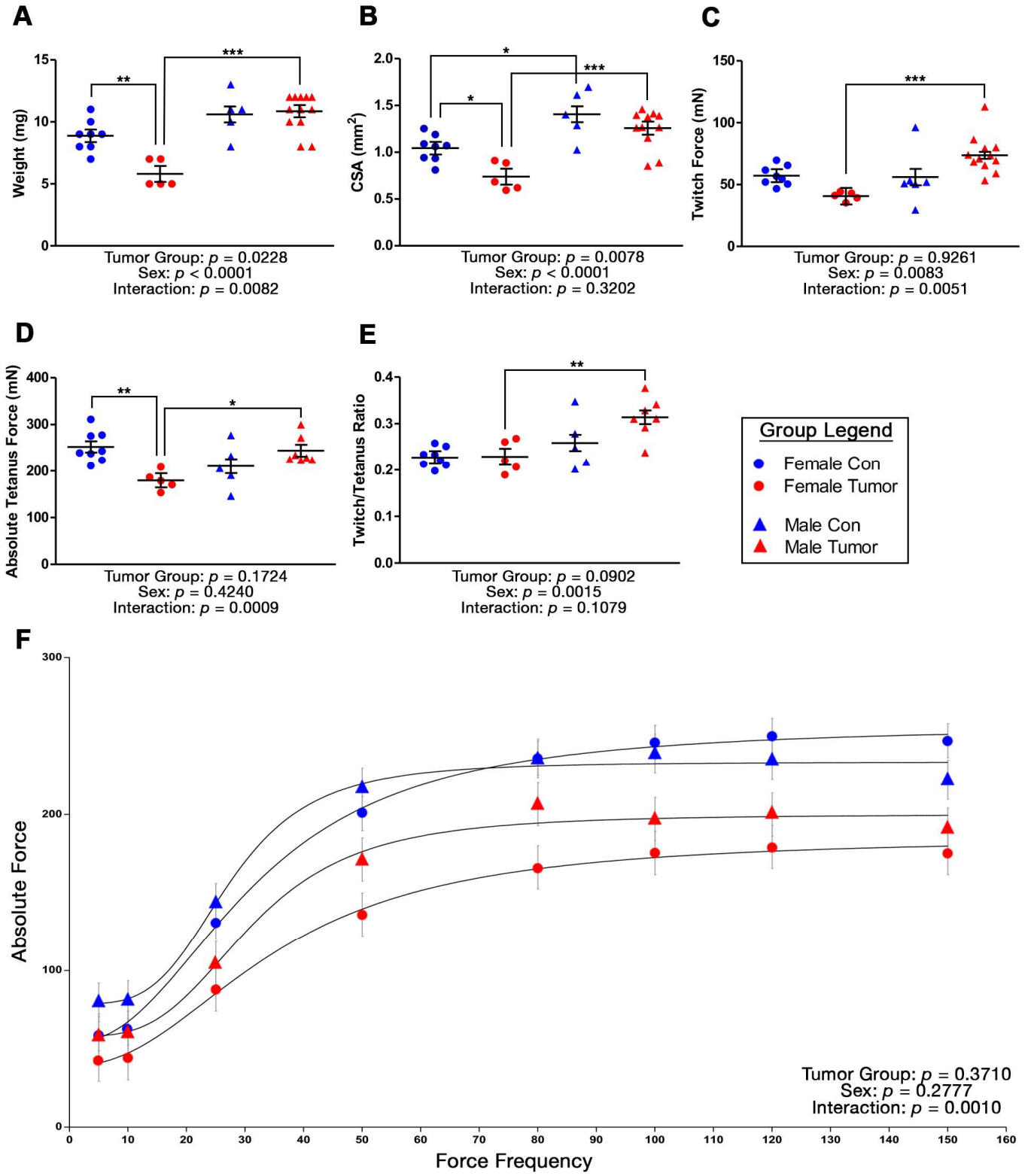

Figure 4. (**A**–**F**). Tumor-induced changes to EDL contractile properties by sex. Mixed models evaluating the effects of sex and tumor group on (**A**) muscle mass, (**B**) cross sectional area (CSA), (**C**) peak twitch force, (**D**) peak tetanus force, (**E**) peak twitch/tetanus ratio, and (**F**) absolute force at various stimulation frequencies of the EDL muscle (n = 5–12 muscles per sample group). Data are presented as least squares means (LSM) ± SE. Significant pairwise differences between groups (**A**–**E**) are denoted as * $p < 0.05$, ** $p < 0.01$, *** $p < 0.001$.

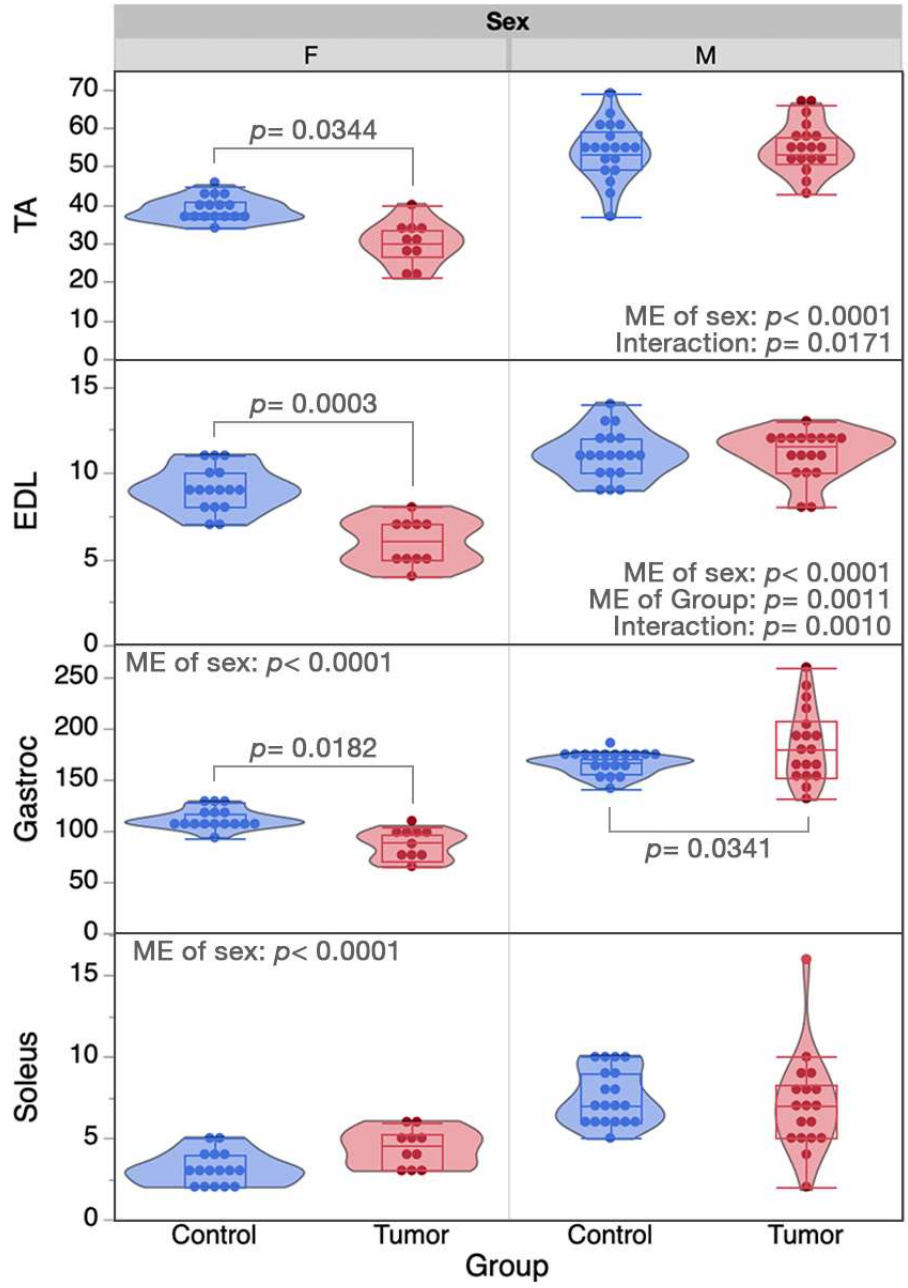

Figure 5. Tumor-induced changes to muscle mass. Data are displayed in violin plots with equal area and quartiles denoted, excluding outliers. Control groups of each sex are represented in blue, and tumor groups represented in red. Significant pairwise differences between groups of each sex are denoted, if they exist. In addition to denoted pairwise differences, the muscle mass of male controls was significantly higher than female controls for all muscles ($p \leq 0.01$) and muscle masses from male tumor mice were higher than female tumor mice for the EDL, TA, and gastrocnemius muscles ($p < 0.0001$) but not the soleus. Sample sizes for each of the four muscles were n = 10–19 muscles for each sample group. EDL, extensor digitorum longus; F, female; M, male; ME, main effect; TA, tibialis anterior.

To address the fatigue properties of isolated skeletal muscle in response to tumor growth in both sexes, the EDL muscle was subjected to a repeated contraction protocol designed to induce loss of force over time. Differences in absolute force production and relative fatiguability between study groups were minimal and primarily reflected function in the first 30 repetitions, with indistinguishable patterns existing thereafter. Fixed effect

statistics for absolute and relative fatigue mixed models can be found in Table S3. The sex*repetition interaction was the only fixed effect for the absolute force model that did not significantly affect force generation ($p = 0.0992$), despite a significant main effect of sex ($p = 0.0191$) and a sex*group*repetition interaction ($p < 0.0001$). These findings suggest that reductions in absolute force generation with repetitive stimulation are not variable based upon sex alone, but that the rate of force reduction is different between male and female tumor mice as compared to their respective controls. Changes to relative force production with repetitive stimulation, or fatiguability, were independently affected by sex (sex*repetition interaction: $p < 0.0001$) and tumor group (group*repetition interaction: $p < 0.0001$); however, the lack of a three-way sex*group*repetition interaction suggests that the rate of skeletal muscle fatiguability differs between males and females, though they are similarly influenced by breast tumor growth.

3. Discussion

In the current study, we utilized female and male PyMT mice to test the hypothesis that the isometric contractile properties and molecular composition of male and female skeletal muscle would be differentially influenced by the development of breast tumors. The PyMT transgenic mouse model allowed the testing of this hypothesis with naturally developing tumors in both male and female mice, which mirror typical clinical timelines of the disease [11]. The data presented herein support our hypothesis, and we identify several biological pathways and muscle functional properties that are differentially regulated in female and male PyMT mice. In addition, our data support the sexual dimorphism of skeletal muscle in general, as several genes in our dataset were previously identified as differentially regulated in female and male skeletal muscle [27]. Collectively, the data presented in this study provide a framework through which the PyMT mouse model of breast cancer can be used to evaluate therapeutic strategies targeting tumor-associated skeletal muscle alterations.

Our laboratory has published data to support the existence of a clinically relevant phenotype of breast cancer-associated muscle fatigue in the absence of cachexia in females [17,18]. Skeletal muscle biopsies from female breast cancer patients and muscles from female mice implanted with patient-derived xenografts from breast tumors (BC-PDOX) showed strikingly similar molecular composition coupled with lower levels of intramuscular ATP [18]. Additionally, muscles from these BC-PDOX mice fatigued at a faster rate compared to non-tumor control mice and sham BC-PDOX mice, with no differences in overall body mass or muscle mass [17]. In the current study, we utilized female PyMT mice that were in the fourth stage of tumor growth, which likely experienced a greater overall tumor burden compared to our prior BC-PDOX mouse model. The skeletal muscles from female PyMT mice investigated in the current study show some similarities to muscles from BC-PDOX mice and suggest a consistent phenotype in association with breast tumor growth. For example, GO pathway analysis of RNA sequencing identified downregulation of many metabolic and mitochondrial function pathways in muscles from female PyMT mice, including oxidative phosphorylation and aerobic respiration. From a muscle function perspective, female PyMT mice herein demonstrated reduced peak tetanus forces, as well as a slower rate of force development and rate of relaxation, consistent with muscles from BC-PDOX mice.

In contrast, there were notable differences in the degree of muscle wasting and muscle fatiguability observed in stage 4 PyMT female mice compared to female BC-PDOX mice. Most importantly, stage 4 female PyMT mice demonstrated muscle wasting across multiple muscles with a type II fiber composition. Specifically, the EDL, TA, and gastrocnemius muscles of females weighed less at euthanasia compared to non-tumor control mice. This lower muscle mass was reflected in the lower absolute force production in the EDL muscle. Muscle wasting was not observed in our prior female BC-PDOX mouse model, despite a greater time exposed to tumor growth compared to PyMT mice. The transgenic PyMT model induces a significant degree of tumor burden in a relatively short period of time [11],

which may be associated with a greater loss of muscle mass in this corresponding time frame. Given the downregulation of mitochondrial and cellular respiration pathways in the muscles of female PyMT mice, it is surprising that we did not observe quantifiable ex vivo muscle fatigue. We speculate that the greater degree of muscle wasting observed in stage 4 female PyMT mice may have contributed to our inability to quantify fatigue with repeated stimulation. MacDougall et al. provide compelling data to suggest that stimulation frequency can have differing effects on force output during low- and high-frequency stimulation, with less force loss observed in response to low-frequency muscle stimulation [28]. The mouse EDL reaches maximum force in response to >120 Hz stimulation [29], while 40 Hz stimulation is utilized for our fatigue protocol [30]. There may be an interplay between frequency/fatigue/potentiation in the setting of advanced cancer, which requires further investigation in a sex-specific manner. Functionally, male tumor mice did not differ from male controls in contractile force, speed, relaxation rates, or fatiguability. Unlike females, the EDL, TA, and soleus muscles did not differ in weight between male tumor mice and controls. Collectively, the data in these two different mouse models of breast cancer suggest that female PyMT mice in stage 4 may better represent patients with metastatic disease, where cachexia is more common [31,32], compared to BC-PDOX mice, which may better represent patients with early-stage disease being treated with curative intent [17].

To our knowledge, this is the first study to assess the sexual dimorphism of skeletal muscle within the PyMT mouse model of breast cancer. Interestingly, clustering of the 2000 most differentially expressed genes demonstrated two key patterns: first, a sex-dependent difference, independent of tumor growth (clusters A and C; Figure 1A, Table 1), and second, dysregulation between the female tumor and control groups that does not differ between male groups. This is coupled with the substantial differences in DEGs, with almost 8000 DEGs identified in the muscles of female PyMT mice, yet only 40 DEGs in males, each compared to their respective controls. These findings suggest that, compared to females, breast tumor growth in male PyMT mice is associated with fewer total dysregulated genes in skeletal muscle and with a lower magnitude of change. Trends in gene expression in response to tumor growth were entirely divergent in males and females. Only 17 pathways were dysregulated in males, all of which reflect increased inflammatory activity; none of these pathways were dysregulated in female mice. Rather, females independently demonstrated upregulation of autophagic and protein synthesis pathways, in addition to downregulation of pathways involving cell metabolism, extracellular membrane structure, and synaptic membranes. Numerous KEGG pathways also reflect substantial gene dysregulation in muscles from female tumor mice that did not exist in males, though a few diverging trends did exist. Muscle contraction pathways demonstrated downregulation of contractile fiber genes, which are instead upregulated in males, while calcium signaling genes were downregulated in female PyMT mice but were relatively unaffected in males. The other key diverging pattern in gene expression between sexes is in inflammatory mechanisms, including antigen processing and presentation pathways and in class I helical cytokine activity. Despite similar expression profiles for the major histocompatibility complex (MHC) I pathway, females experienced a general downregulation of the MHC II pathway, while males experienced a general upregulation (Figure 3A,B). Further, directional changes in response to tumor growth differed by sex in γ-chain-utilizing and IL-6/IL-12-like cytokine interactions; many γ-chain-utilizing cytokines were downregulated in response to tumor growth in female skeletal muscle, while they were upregulated in males (Figure S1A,C).

This PyMT model of breast cancer provides an opportunity to model the sex differences that clinically parallel the disease. Current standards for routine screenings, in addition to therapeutic advancements, have contributed to the high rates of success for early detection of breast cancer in females. Given the rarity of the disease in males, and thus lack of routine screening standards, late-stage detection of the disease is more common [3,4]. Our prior research suggests that measurable changes in female skeletal muscle occur during early-stage disease [17,18]; the present study was designed with consideration of the differential

diagnostic timelines for male patients to enhance its clinical applicability. In addition to evaluating late-stage disease, the PyMT model also presents similarities in the molecular classification of tumors common to male breast cancer. The clinical presentation of male breast tumors almost exclusively represents ER-positive tumors of the luminal subtype; specifically, the luminal B subtype exhibited by the PyMT model has been reported as the most common molecular subtype for male breast cancer [33]. The role of estrogen in acute stress responses could play a part in these sexually dimorphic trends. Lower estrogen levels may reduce free radical oxidation (i.e., ROS), reduce plasma membrane stability, enhance immune cell infiltration, and reduce downstream activation of satellite cells [34]. Differences in hormonal effects suggest the potential for differing responses to tumor-induced hormonal changes, as well as differing responses to clinical treatment methods. The data herein suggest that breast-tumor-induced changes to skeletal muscle are mediated by separate mechanisms and differentially affect function. The maladaptation of female muscle is likely in response to metabolic stress, leading to the inability to effectively repair cellular damage. In contrast, male muscle is likely more resistant to metabolic reprogramming in this manner due to dimorphic variations in the resting metabolism [35]; thus, adaptations occurring in male muscle may exist in response to acute stress, of a different origin, to further develop an inflammation-mediated mechanism of maladaptation.

It should be noted that a limitation of the present study is the potential influence of aging; given the sex differences in tumor development in the PyMT mouse model, it is unknown whether aging combined with tumor burden has a differential impact on skeletal muscle. Clinically, however, males tend to present with larger primary tumor sizes and obtain diagnoses at a later age compared to women [36]. Future research should continue to explore the influence of breast tumors on skeletal muscle in the PyMT mouse model, including tumor stage and sex differences. Our laboratory is currently working to develop PYMT tumor xenografts in both male and female mice in an attempt to age-match groups; this model will allow replication of the present study in the absence of potential age-related confounds. In summary, the data herein support the hypothesis that the contractile properties and molecular composition of male and female skeletal muscles differ and are likely influenced by the temporal differences in tumor growth between the sexes. In addition, our data support the sexual dimorphism of skeletal muscle in general and in response to tumor growth. Collectively, the data presented herein provide a framework through which the PyMT mouse model of breast cancer can be used to evaluate therapeutic strategies targeting tumor-associated skeletal muscle alterations.

4. Materials and Methods

4.1. Animals

MMTV-PyMT FVB/NJ mice are a model of breast cancer in which the polyoma virus middle T oncoprotein (PyMT) is under the control of the mouse mammary tumor virus (MMTV) promoter [11]. Female and male PyMT$^+$ and littermate control mice (FVB/N-Tg(MMTV-PyVT)634Mul/J, strain # 002374) were obtained from a breeding colony maintained at West Virginia University, originally procured from Jackson Laboratory (The Jackson Laboratory, Bar Harbor, ME, USA). Female PyMT$^+$ mice and sex-matched littermate control mice were used for experiments at approximately 16 weeks of age, which corresponds with stage 4 disease [11]. Male PyMT$^+$ mice between 6 and9 months of age were used for experiments. These ages in female and male mice represent the time for maximal tumor burden (Figure S5) and also reflect the sexual dimorphism of tumor initiation and growth within this mouse strain. Four study groups were utilized as follows: female control (FC); female tumor (FT); male control (MC); male tumor (MT). Group sample sizes for all variables are provided in Table S2. Mice were housed in the animal vivarium at West Virginia University at 22 °C under a 12:12 h light/dark cycle and received food and water ad libitum. Rodent chow was an irradiated global 18% protein rodent diet free of phytoestrogens (2018 Teklad; Inotiv, West Lafayette, IN, USA). All animal experiments were approved by the Institutional Animal Care and Use Committee at West Virginia University.

4.2. Ex Vivo Muscle Physiological Analysis

Mice were anesthetized with isoflurane prior to the dissection of the bilateral tibialis anterior (TA), extensor digitorum longus (EDL), gastrocnemius, and soleus muscles. Isometric contractile properties were examined in the EDL muscles ex vivo, using established laboratory methodology [37,38]. Briefly, EDL muscles were transferred independently to an oxygenated muscle stimulation bath containing Ringer's solution (100 mM NaCl, 4.7 mM KCl, 3.4 mM $CaCl_2$, 1.2 mM KH_2PO_4, 1.2 mM $MgSO_4$, 25 mM HEPES, and 5.5 mM D-glucose) that was maintained at 22 °C. Muscle stimulation was performed using a commercially available muscle physiology system (Aurora Scientific, Aurora, ON, Canada). EDL muscle length was gradually increased to obtain the maximal twitch force response; this muscle length was recorded as optimal length (L_o). Muscle contractile parameters obtained from isometric twitch contractions included peak isometric twitch force, contraction time (CT), $\frac{1}{2}$ relaxation time ($\frac{1}{2}$ RT), rate of force development (RFD), and rate of relaxation (RR).

With the muscle set at L_o, muscles were stimulated with 500ms tetanic trains at increasing frequencies (i.e., 5, 10, 25, 50, 80, 100, 120, and 150 Hz) to establish the force–frequency relationship. Each contraction was followed by 2 min rest. Absolute isometric tetanic force was recorded at each stimulation frequency; nonlinear regression was used to generate a sigmoid curve relating this muscle force (P) to stimulation frequency (f) using Equation (1) [39]:

$$P = P_{min} + \frac{P_{max} - P_{min}}{1 + \left(\frac{K_f}{f}\right)^h} \quad (1)$$

The following parameters were obtained from the force–frequency curve: minimum force (P_{min}), maximum force (P_{max}), half-frequency (K_f), and the Hill coefficient (h). K_f is defined as the frequency at which the developed force is the midpoint between P_{min} and P_{max}, where h is defined as the slope of the force–frequency sigmoidal curve [39].

Muscle fatigue was analyzed using repeated 40 Hz tetanic trains that occurred once per second and lasted 330ms, for a total of 6 min [37]. Muscle cross-sectional area (CSA) was calculated by dividing the muscle mass by the product of the muscle density coefficient (1.06 g·cm^3), muscle L_o, and the fiber length coefficient (EDL: 0.45); this CSA value was used to calculate muscle-specific force (i.e., force mN·muscle CSA^{-1}) [29,40].

4.3. RNA Isolation, Sequencing, and Bioinformatics

Bulk RNA was isolated from TA muscles of five mice from each of the four treatment groups (n = 20) using Trizol (ThermoFisher Scientific, Waltham, MA, USA) and established methods [41]. A NanoDrop spectrophotometer was used to determine RNA purity, with 260/280 readings of at least 2.0. RNA integrity was quantified on an Agilent bioanalyzer with an RNA Nano chip. RNA samples had RNA integrity numbers (RIN) > 9, suggesting high-quality RNA. A KAPA Stranded mRNA kit was used to build RNA-Seq libraries at the West Virginia University Genomics Core Facility. The libraries were sent to the Marshall University Genomics Core and were sequenced with a NextSeq 2000 on a P2 100 cycle flowcell (PE50bp). (BioProject ID: PRJNA974704 murine samples). Subsequently, the paired reads were aligned to the GRCm39.109 mouse reference genome utilizing HISAT2 (version 2.2.1) [42]. The 20 RNA samples averaged 24.9 ± 2.5 million reads per sample with a 95.8 ± 1.4% mapping rate to the GRCm39.109 genome. Raw gene counts were generated with the htseq-count function of HTSeq (version 2.0.2) [43].

RNA sequencing analyses of raw gene counts were completed using the iDEP.96 web application [44]. An EdgeR logarithmic transform was applied to raw counts prior to k-means clustering and principal components analysis (PCA). The k-means clustering analysis was performed using the mean center of the 2000 most variable genes across all study groups. Four clusters were used to categorize genes based upon the diminished within-group sum of squares. The genes in each cluster were then used to identify differentially regulated gene ontology (GO) pathways (biological process, cellular component, and

molecular function). The PCA was performed on gene covariance across the samples for representation of group variability. Correlations between sample eigenvectors of each principal component (PC) and main factors of sex (male vs. female) and group (control vs. tumor) were investigated.

Further, differentially expressed genes (DEGs) were identified across the four groups using the DESeq2 method, with a false discovery rate (FDR) cutoff of 0.1 and a minimum fold change of 1. The GAGE method was used for functional enrichment analysis to identify the most differentially expressed GO pathways with an FDR of 0.05 (Biological Process, Cellular Component, and Molecular Function) [45]. Specific KEGG pathways were also evaluated for representation of gene expression in tumor vs. control mice for each sex [46,47].

In total, 17,461 genes had at least one sample with a read count above zero and were included in RNA sequencing analyses. Control samples of this coisogenic mouse model (n = 10) had an average coefficient of variation (CV) of 45% (FC CV = 39.80%, MC CV = 34.86%) for all genes. Post hoc power analyses indicated a power of 0.80 for a sample size of five mice per group, with model variance of 45% and an FDR of 0.1 [48].

4.4. Statistical Analyses

Statistical analyses were run using JMP Pro (version 16.0.0). Muscle contractile properties and mass measurements were evaluated using 2-way ANOVA mixed models with main effects of sex (male vs. female) and tumor group (control vs. tumor), as well as the interaction between the two main effects. For fatigue and force–frequency analyses, linear mixed effect models were used with an additional main effect of repetition or frequency, respectively, as well as sex, group, and all interaction effects. All variables were checked for homogeneity of variance between study groups using Levene's test; variables determined to have equal variance were run with a residual mixed model structure, while those determined to be heterogeneous variance were run with an unequal variance structure. For variables in which numerous measurements may have been recorded from the same mouse (i.e., muscle weights from the left and right legs), a random effect of mouse was applied to account for intra-sample variability.

Tukey's honestly significant difference test (HSD) was utilized to correct for multiple comparisons and determine significant pairwise differences within each model. An alpha level of $p < 0.05$ was used to determine the significance of fixed effects and pairwise comparisons.

Supplementary Materials: The following supporting information can be downloaded at: https://www.mdpi.com/article/10.3390/ijms241411669/s1.

Author Contributions: Conceptualization, S.A.C., A.D.M., E.E.P., L.E.R. and M.A.W.; methodology, S.A.C., I.H., A.D.M., E.E.P., L.E.R. and M.A.W.; validation, S.A.C., A.D.M. and L.E.R.; formal analysis, S.A.C., M.G.C., I.H., A.D.M. and L.E.R.; resources, E.E.P., T.D.E. and E.H.H.; data curation, S.A.C., M.G.C., A.D.M., L.E.R. and M.A.W.; writing—original draft preparation, E.E.P., L.E.R. and M.A.W.; writing—review and editing, S.A.C., A.D.M., E.E.P., L.E.R. and M.A.W.; visualization, I.H. and L.E.R.; supervision, E.E.P.; project administration, E.E.P. and M.A.W.; funding acquisition, E.E.P. All authors have read and agreed to the published version of the manuscript.

Funding: This research was supported by the following organizations: National Institutes of Arthritis, Musculoskeletal and Skin Diseases (NIAMS) under award number R01AR079445 (Pistilli); National Institutes of General Medical Sciences under award number P20GM121322 (Lockman); National Cancer Institute under award numbers R01CA194013 and R01CA192064 (Eubank); the WVU Genomics Core Facility (U54GM104942); the Marshall University Genomics Core Facility (P20GM103434; 1P20GM121299).

Institutional Review Board Statement: The animal study protocol was approved by the Institutional Animal Care and Use Committee at West Virginia University (1603001124, date of approval—8 September 2020).

Informed Consent Statement: Not applicable.

Data Availability Statement: Raw sequencing data presented in this study are openly available on BioProject (ID: PRJNA974704 murine samples).

Acknowledgments: The authors wish to acknowledge the WVU undergraduate interns involved in this project (Steven Blume, Jana Hatfield, Ty-Angelo Giorcelli, Sarah Palmer).

Conflicts of Interest: The authors declare no conflict of interest.

References

1. *Cancer Facts & Figures 2023*; American Cancer Society: Atlanta, GA, USA, 2023.
2. White, J.; Kearins, O.; Dodwell, D.; Hogan, K.; Hanby, A.M.; Speirs, V. Male breast carcinoma: Increased awareness needed. *Breast Cancer Res.* **2011**, *13*, 219. [CrossRef] [PubMed]
3. Liu, N.; Johnson, K.J.; Ma, C.X. Male Breast Cancer: An Updated Surveillance, Epidemiology, and End Results Data Analysis. *Clin. Breast Cancer* **2018**, *18*, e997–e1002. [CrossRef]
4. Sosa Rivera, A.M.; Espinoza, S.L.; Aguilar, R.M.; Palencia, R. Male Breast Cancer: Case Report. *Rev. Colomb. Cardiol.* **2017**, *28*, 4810–4815.
5. Maglione, J.E.; Moghanaki, D.; Young, L.J.T.; Manner, C.K.; Ellies, L.G.; Joseph, S.O.; Nicholson, B.; Cardiff, R.D.; MacLeod, C.L. Transgenic *Polyoma Middle-T* Mice Model Premalignant Mammary Disease. *Cancer Res.* **2001**, *61*, 8298–8305. [PubMed]
6. Shishido, S.; Delahaye, A.; Beck, A.; Nguyen, T.A. The MMTV-PyVT Trangenic Mouse as a Multistage Model for Mammary Carcinoma and the Efficacy of Antineoplastic Treatment. *J. Cancer Ther.* **2013**, *4*, 1187–1197. [CrossRef]
7. Attalla, S.; Taifour, T.; Bui, T.; Muller, W. Insights from transgenic mouse models of PyMT-induced breast cancer: Recapitulating human breast cancer progression in vivo. *Oncogene* **2021**, *40*, 475–491. [CrossRef] [PubMed]
8. Fantozzi, A.; Christofori, G. Mouse models of breast cancer metastasis. *Breast Cancer Res.* **2006**, *8*, 212. [CrossRef]
9. Park, M.K.; Lee, C.H.; Lee, H. Mouse models of breast cancer in preclinical research. *Lab. Anim. Res.* **2018**, *34*, 160–165. [CrossRef]
10. Regua, A.T.; Arrigo, A.; Doheny, D.; Wong, G.L.; Lo, H.-W. Transgenic mouse models of breast cancer. *Cancer Lett.* **2021**, *516*, 73–83. [CrossRef]
11. Lin, E.Y.; Jones, J.G.; Li, P.; Zhu, L.; Whitney, K.D.; Muller, W.J.; Pollard, J.W. Progression to malignancy in the polyoma middle T oncoprotein mouse breast cancer model provides a reliable model for human diseases. *Am. J. Pathol.* **2003**, *163*, 2113–2126. [CrossRef]
12. Fluck, M.M.; Schaffhausen, B.S. Lessons in Signaling and Tumorigenesis from Polyomavirus Middle T Antigen. *Microbiol. Mol. Biol. Rev.* **2009**, *73*, 542–563. [CrossRef] [PubMed]
13. Yan, L.; Sundaram, S.; Rust, B.M.; Picklo, M.J.; Bukowski, M.R. Mammary Tumorigenesis and Metabolome in Male Adipose Specific Monocyte Chemotactic Protein−1 Deficient MMTV-PyMT Mice Fed a High-Fat Diet. *Front. Oncol.* **2021**, *11*, 667843. [CrossRef] [PubMed]
14. Fearon, K.C.; Glass, D.J.; Guttridge, D.C. Cancer Cachexia: Mediators, Signaling, and Metabolic Pathways. *Cell Metab.* **2012**, *16*, 153–166. [CrossRef] [PubMed]
15. Evans, W.J.; Lambert, C.P. Physiological Basis of Fatigue. *Am. J. Phys. Med. Rehabil.* **2007**, *86*, S29–S46. [CrossRef]
16. Baracos, V.E.; Martin, L.; Korc, M.; Guttridge, D.C.; Fearon, K.C.H. Cancer-associated cachexia. *Nat. Rev. Dis. Primers* **2018**, *4*, 17105. [CrossRef]
17. Wilson, H.E.; Rhodes, K.K.; Rodriguez, D.; Chahal, I.; Stanton, D.A.; Bohlen, J.; Davis, M.; Infante, A.M.; Hazard-Jenkins, H.; Klinke, D.J.; et al. Human Breast Cancer Xenograft Model Implicates Peroxisome Proliferator–activated Receptor Signaling as Driver of Cancer-induced Muscle Fatigue. *Clin. Cancer Res.* **2019**, *25*, 2336–2347. [CrossRef] [PubMed]
18. Wilson, H.E.; Stanton, D.A.; Montgomery, C.; Infante, A.M.; Taylor, M.; Hazard-Jenkins, H.; Pugacheva, E.N.; Pistilli, E.E. Skeletal muscle reprogramming by breast cancer regardless of treatment history or tumor molecular subtype. *NPJ Breast Cancer* **2020**, *6*, 18. [CrossRef]
19. Cella, D.; Lai, J.S.; Chang, C.H.; Peterman, A.; Slavin, M. Fatigue in cancer patients compared with fatigue in the general United States population. *Cancer* **2002**, *94*, 528–538. [CrossRef]
20. Curt, G.A.; Breitbart, W.; Cella, D.; Groopman, J.E.; Horning, S.J.; Itri, L.M.; Johnson, D.H.; Miaskowski, C.; Scherr, S.L.; Portenoy, R.K.; et al. Impact of cancer-related fatigue on the lives of patients: New findings from the Fatigue Coalition. *Oncologist* **2000**, *5*, 353–360. [CrossRef]
21. Bower, J.E.; Ganz, P.A.; Desmond, K.A.; Rowland, J.H.; Meyerowitz, B.E.; Belin, T.R. Fatigue in Breast Cancer Survivors: Occurrence, Correlates, and Impact on Quality of Life. *J. Clin. Oncol.* **2000**, *18*, 743–753. [CrossRef]
22. Thong, M.S.Y.; van Noorden, C.J.F.; Steindorf, K.; Arndt, V. Cancer-Related Fatigue: Causes and Current Treatment Options. *Curr. Treat. Options Oncol.* **2020**, *21*, 17. [CrossRef] [PubMed]
23. Mustian, K.M.; Alfano, C.M.; Heckler, C.; Kleckner, A.S.; Kleckner, I.R.; Leach, C.R.; Mohr, D.; Palesh, O.G.; Peppone, L.J.; Piper, B.F.; et al. Comparison of Pharmaceutical, Psychological, and Exercise Treatments for Cancer-Related Fatigue: A Meta-analysis. *JAMA Oncol.* **2017**, *3*, 961–968. [CrossRef] [PubMed]
24. Zhong, X.; Zimmers, T.A. Sex Differences in Cancer Cachexia. *Curr. Osteoporos. Rep.* **2020**, *18*, 646–654. [CrossRef]
25. Montalvo, R.N.; Counts, B.R.; Carson, J.A. Understanding Sex Differences in the Regulation of Cancer-Induced Muscle Wasting. *Curr. Opin. Support. Palliat. Care* **2018**, *12*, 394–403. [CrossRef] [PubMed]

26. Wilson, H.E.; Stanton, D.A.; Rellick, S.; Geldenhuys, W.; Pistilli, E.E. Breast cancer-associated skeletal muscle mitochondrial dysfunction and lipid accumulation is reversed by PPARG. *Am. J. Physiol. Cell Physiol.* **2021**, *320*, C577–C590. [CrossRef] [PubMed]
27. O'Reilly, J.; Ono-Moore, K.D.; Chintapalli, S.V.; Rutkowsky, J.M.; Tolentino, T.; Lloyd, K.C.K.; Olfert, I.M.; Adams, S.H. Sex differences in skeletal muscle revealed through fiber type, capillarity, and transcriptomics profiling in mice. *Physiol. Rep.* **2021**, *9*, e15031. [CrossRef]
28. MacDougall, K.B.; Devrome, A.N.; Kristensen, A.M.; MacIntosh, B.R. Force-frequency relationship during fatiguing contractions of rat medial gastrocnemius muscle. *Sci. Rep.* **2020**, *10*, 11575. [CrossRef]
29. Brooks, S.V.; Faulkner, J.A. Contractile properties of skeletal muscles from young, adult and aged mice. *J. Physiol.* **1988**, *404*, 71–82. [CrossRef]
30. Burke, R.E.; Levine, D.N.; Tsairis, P.; Zajac, F.E., 3rd. Physiological types and histochemical profiles in motor units of the cat gastrocnemius. *J. Physiol.* **1973**, *234*, 723–748. [CrossRef]
31. Biswas, A.K.; Acharyya, S. Understanding cachexia in the context of metastatic progression. *Nat. Rev. Cancer* **2020**, *20*, 274–284. [CrossRef]
32. Fearon, K.; Arends, J.; Baracos, V. Understanding the mechanisms and treatment options in cancer cachexia. *Nat. Rev. Clin. Oncol.* **2013**, *10*, 90–99. [CrossRef] [PubMed]
33. Sánchez-Muñoz, A.; Vicioso, L.; Santonja, A.; Álvarez, M.; Plata-Fernández, Y.; Miramón, J.; Zarcos, I.; Ramírez-Tortosa, C.L.; Montes-Torres, J.; Jerez, J.M.; et al. Male breast cancer: Correlation between immunohistochemical subtyping and PAM50 intrinsic subtypes, and the subsequent clinical outcomes. *Mod. Pathol.* **2018**, *31*, 299–306. [CrossRef]
34. Enns, D.L.; Tiidus, P.M. The influence of estrogen on skeletal muscle: Sex matters. *Sports Med.* **2010**, *40*, 41–58. [CrossRef]
35. Rubin, J.B.; Lagas, J.S.; Broestl, L.; Sponagel, J.; Rockwell, N.; Rhee, G.; Rosen, S.F.; Chen, S.; Klein, R.S.; Imoukhuede, P.; et al. Sex differences in cancer mechanisms. *Biol. Sex Differ.* **2020**, *11*, 17. [CrossRef] [PubMed]
36. Anderson, W.F.; Jatoi, I.; Tse, J.; Rosenberg, P.S. Male breast cancer: A population-based comparison with female breast cancer. *J. Clin. Oncol.* **2010**, *28*, 232–239. [CrossRef] [PubMed]
37. Pistilli, E.E.; Bogdanovich, S.; Garton, F.; Yang, N.; Gulbin, J.P.; Conner, J.D.; Anderson, B.G.; Quinn, L.S.; North, K.; Ahima, R.S.; et al. Loss of IL−15 receptor α alters the endurance, fatigability, and metabolic characteristics of mouse fast skeletal muscles. *J. Clin. Investig.* **2011**, *121*, 3120–3132. [CrossRef]
38. Pistilli, E.E.; Alway, S.E.; Hollander, J.M.; Wimsatt, J.H. Aging alters contractile properties and fiber morphology in pigeon skeletal muscle. *J. Comp. Physiol. B* **2014**, *184*, 1031–1039. [CrossRef]
39. Kiriaev, L.; Kueh, S.; Morley, J.W.; Houweling, P.J.; Chan, S.; North, K.N.; Head, S.I. Dystrophin-negative slow-twitch soleus muscles are not susceptible to eccentric contraction induced injury over the lifespan of the *mdx* mouse. *Am. J. Physiol. Cell Physiol.* **2021**, *321*, C704–C720. [CrossRef]
40. Lynch, G.S.; Hinkle, R.T.; Chamberlain, J.S.; Brooks, S.V.; Faulkner, J.A. Force and power output of fast and slow skeletal muscles from mdx mice 6−28 months old. *J. Physiol.* **2001**, *535*, 591–600. [CrossRef]
41. Pistilli, E.E.; Jackson, J.R.; Alway, S.E. Death receptor-associated pro-apoptotic signaling in aged skeletal muscle. *Apoptosis* **2006**, *11*, 2115–2126. [CrossRef]
42. Kim, D.; Paggi, J.M.; Park, C.; Bennett, C.; Salzberg, S.L. Graph-based genome alignment and genotyping with HISAT2 and HISAT-genotype. *Nat. Biotechnol.* **2019**, *37*, 907–915. [CrossRef] [PubMed]
43. Putri, G.H.; Anders, S.; Pyl, P.T.; Pimanda, J.E.; Zanini, F. Analysing high-throughput sequencing data in Python with HTSeq 2.0. *Bioinformatics* **2022**, *38*, 2943–2945. [CrossRef]
44. Ge, S.X.; Son, E.W.; Yao, R. iDEP: An integrated web application for differential expression and pathway analysis of RNA-Seq data. *BMC Bioinform.* **2018**, *19*, 534. [CrossRef] [PubMed]
45. Luo, W.; Friedman, M.S.; Shedden, K.; Hankenson, K.D.; Woolf, P.J. GAGE: Generally applicable gene set enrichment for pathway analysis. *BMC Bioinform.* **2009**, *10*, 161. [CrossRef] [PubMed]
46. Luo, W.; Brouwer, C. Pathview: An R/Bioconductor package for pathway-based data integration and visualization. *Bioinformatics* **2013**, *29*, 1830–1831. [CrossRef] [PubMed]
47. Kanehisa, M.; Furumichi, M.; Sato, Y.; Ishiguro-Watanabe, M.; Tanabe, M. KEGG: Integrating viruses and cellular organisms. *Nucleic Acids Res.* **2021**, *49*, D545–D551. [CrossRef]
48. Hart, S.; Therneau, T.; Zhang, Y.; Poland, G.; Kocher, J. Calculating Sample Size Estimates for RNA Sequencing Data. *J. Comput. Biol.* **2013**, *20*, 970–978. [CrossRef]